


# Band Anticrossing in Dilute Germanium Carbides Using Hybrid Density Functionals

CHAD A. STEPHENSON <sup>1,3</sup> WILLIAM A. O'BRIEN,<sup>1</sup> MENG QI,<sup>1</sup>  
MICHAEL PENNINGER,<sup>2</sup> WILLIAM F. SCHNEIDER,<sup>2</sup>  
and MARK A. WISTEY<sup>1</sup>

1.—Department of Electrical Engineering, University of Notre Dame, Notre Dame, IN 46556, USA. 2.—Department of Chemical and Biomolecular Engineering, University of Notre Dame, Notre Dame, IN 46556, USA. 3.—e-mail: stephenson.15@nd.edu

Dilute germanium carbides ( $\text{Ge}_{1-x}\text{C}_x$ ) offer a direct bandgap for compact silicon photonics, but widely varying properties have been reported. This work reports improved band structure calculations for  $\text{Ge}_{1-x}\text{C}_x$  using *ab initio* simulations that employ the HSE06 exchange–correlation density functional. Contrary to Vegard's law, the conduction band minimum at  $\Gamma$  is consistently found to decrease with increasing C content, while *L* and *X* valleys change much more slowly. The calculated Ge bandgap is within 11% of experimental values. A decrease in energy at the  $\Gamma$  conduction band valley of  $(170 \text{ meV} \pm 50)/\%C$  is predicted, leading to a direct bandgap for  $x > 0.008$ . These results indicate a promising material for Group IV lasers.

**Key words:** Germanium, germanium carbon, density functional theory, hybrid functionals

## INTRODUCTION

Even though the size of transistors has continued to decrease, the clock speed of Si complementary metal oxide semiconductor (CMOS) chips has stagnated, while the number of central processing unit (CPU) cores per computer is increasing exponentially. Photonic integrated circuits provide the necessary bandwidth for long distance data, but input/output (I/O), inter-core, and ultimately memory buses require considerably higher integration of all components within the logic chip itself. Si CMOS lacks an efficient, chemically-compatible laser source.

Ge and Ge alloys have received much attention due to their compatibility with Si and recent demonstrations of enhanced light emission. Liu et al.<sup>1</sup> demonstrated an optically-pumped Ge laser using small amounts of biaxial tensile strain and heavy *n*-type doping, with electroluminescence reported by other groups using similar techniques,<sup>2–4</sup> ultimately yielding an electrically-pumped laser.<sup>5</sup> However, the

very large threshold current of the modestly strained Ge lasers and the fragility of highly strained Ge<sup>6</sup> make the Ge laser impractical for an efficient, integrated light emitter. GeSn has also been heavily investigated as a possible direct bandgap alloy, either as a thick metamorphic layer or grown on metamorphic InGaAs,<sup>7–10</sup> but device lifetimes to date have been limited.

Although both Ge and diamond emit light very weakly due to their indirect bandgap, dilute  $\text{Ge}_{1-x}\text{C}_x$  alloys offer a promising route to creating lasers directly within conventional CMOS electronics.  $\text{Ge}_{1-x}\text{C}_x$  is a highly-mismatched alloy; C is much more electronegative and smaller than Ge, similar to N in the GaInAsN alloy.<sup>11,12</sup> The N (or C) introduces an isoelectronic impurity level near the bottom of the conduction band. Due to the Pauli exclusion principle, the conduction band and impurity level cannot occupy the same energy and repel each other, splitting the conduction band into two bands ( $E^+$  and  $E^-$ ) and driving the  $E^-$  band to lower energy, reducing the bandgap. This is known as the band anticrossing (BAC) model.<sup>11</sup> Although Ge is an indirect bandgap material, the direct ( $\Gamma$ ) conduction

band valley is only 140 meV above the indirect valley. Due to similar s-like (spherical) wavefunction symmetry at the  $\Gamma$  valley, the impurity level is expected to repel the conduction band more strongly at  $\Gamma$  than at  $L$ , turning  $\text{Ge}_{1-x}\text{C}_x$  into a direct bandgap material. The sharp decrease in energy at  $\Gamma$  makes it likely that  $\text{Ge}_{1-x}\text{C}_x$  alloy lasers will emit in the 2–4  $\mu\text{m}$  wavelength range. This energy is less than half of the Si bandgap, which eliminates two-photon absorption in Si waveguides and allows for very efficient light propagation even in high power, high fanout data buses. In addition, an efficient, on-chip, mid-infrared (MIR) laser source is also attractive for gas spectrometry, with several atmospheric transmission windows and many gas absorption lines in this wavelength range.

Strong band bowing has been observed in  $\text{Ge}_{1-x}\text{C}_x$  alloys with very dilute amounts of C.<sup>13</sup> Kolodzey et al. even predicted a direct bandgap alloy region with  $0.04 \leq x \leq 0.11$ .<sup>14</sup> However, others have reported linear increases in bandgap with C incorporation.<sup>15</sup> Differences between experimental results likely stem from defects in the material, particularly interstitial C and C–C clusters. Gall et al. has shown that it is much more energetically favorable for C to form nanoclusters than bond solely to Ge, in contrast to  $\text{Si}_{1-x}\text{C}_x$  alloys.<sup>16</sup> Such defects raise doubts about parameter extraction for semi-empirical and simplified computational models.<sup>17–19</sup>

This work seeks to increase the accuracy of ab initio modeling of defect-free  $\text{Ge}_{1-x}\text{C}_x$  alloys in order to extract their fundamental, intrinsic material properties, as well as to determine a target range of compositions suitable for direct bandgap devices. We use hybrid functionals with and without spin-orbit coupling (SOC) to probe the band structure at C concentrations from 0.78% to 6.25%. As discussed below, the combination of small bandgap and highly-mismatched atoms invalidates many of the approximations that are typically used to reduce computational time in such simulations.

## METHODS

Density functional theory (DFT) calculations were performed using the Vienna ab initio simulation package (VASP),<sup>20–23</sup> the projector-augmented wave (PAW) core treatment and a plane wave basis set with cutoff energy of 400 eV. We used the PAW GGA-PBE<sup>24–27</sup> core model along with HSE06 range separated hybrid exchange–correlation functional.<sup>28</sup> The local density approximation (LDA) is known to underestimate the Ge bandgap to the extent that a semimetal is predicted. Although the generalized gradient approximation (GGA) is one of the most commonly used functionals for bulk materials, it similarly fails to reproduce the Ge band structure, as shown in Fig. 1a. The degeneracy of the valence bands is destroyed because the conduction band has dropped so far that it crosses and

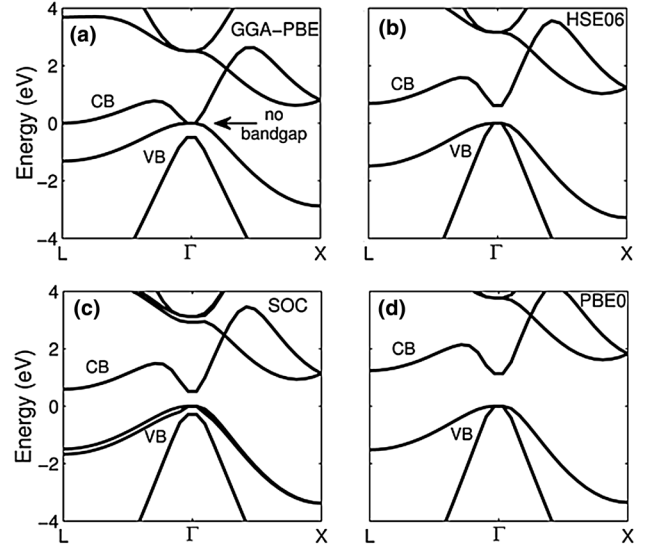


Fig. 1. Validation of choice of modeling technique: 2-atom Ge VASP band structure calculated by (a) the standard DFT GGA-PBE functionals, which grossly underestimate the bandgap to the point of making Ge a semimetal, (b) adding hybrid exchange with HSE06, which opens a bandgap close to experimental values but still has inaccurate degenerate valence bands, (c) including spin-orbit coupling (SOC), which mostly improves valence band modeling by breaking degeneracy, and (d) PBE0 without SOC, accurate but computationally prohibitive.

splits the valence bands. However, by including some of the exact Hartree–Fock exchange through the use of hybrid functionals, a bandgap that closely matches experimental values can be opened up in Ge (Fig. 1b). HSE06 is a more elaborate model that both introduces exact exchange to improve predictions of band gaps and a range separation of this exchange to improve computational efficiency, giving very similar results to more computationally expensive methods such as PBE0 (Fig. 1d) and Green’s function (GW) methods. We also included SOC where feasible for a more accurate representation of the valence bands and the band interactions therein (Fig. 1c). Without SOC, the conduction bands are still well described, especially near the bottom of the valleys, but the splitting in the valence bands cannot be accurately included.

We modeled  $\text{Ge}_{1-x}\text{C}_x$  using periodic 16, 54, and 128-atom supercells in a diamond fcc lattice. These were composed of the 2-atom Ge primitive unit cell repeated 2, 3, and 4 times, respectively, along each basis vector. In each supercell, one Ge atom was replaced with a C atom. We used Gaussian smearing with  $\text{Sigma} = 0.05$  and a  $9 \times 9 \times 9$   $\Gamma$ -centered k-point mesh for the 2-atom cell, which was scaled to  $5 \times 5 \times 5$ ,  $3 \times 3 \times 3$ , and  $1 \times 1 \times 1$  for the 16-atom, 54-atom, and 128-atom supercells, respectively. In each case, the ion locations were first relaxed within the GGA. The lattice constant was then varied using fixed fractional coordinates using the HSE06 potential to minimize system energy.

**Table I. HSE06 computational lattice constants and conduction band edge energies for the  $L$  and  $\Gamma$  high symmetry  $k$  points and minimum in the  $X$  direction with valence band maximum = 0 as reference**

Band edge energies (eV)					
%C	SOC	$L$	$\Gamma$	$X$ min	$a$ (Å)
0	Expmt	0.66	0.8	0.85	5.658
0.00	Yes	0.59	0.517	0.9355	5.6953
0.78	No	0.784	0.3851	1.183	5.6854
1.85	No	0.526	-0.0886	1.057	5.6619
6.25	No	0.651	-0.4988	0.530	5.5744
6.25	Yes	0.625	-0.1875	0.530	5.5744

Experimental values from Ref. 31.

Results are shown in Table I. The lattice constant varies approximately  $-2\%$  from Ge to the highest C fraction.

Figure 1 shows the band structure of 2-atom Ge using PBE, HSE06, and HSE06 + SOC. Figure 1c shows reasonably good fit to Ge experimental results with a slightly underestimated bandgap of 0.59 eV at  $L$  and 0.517 eV at  $\Gamma$  and spin-orbit splitting of 0.283 eV, validating our choice of HSE06 and SOC. These results could be further improved by including the semi-core d electrons as valence electrons rather than part of the core pseudopotential. However, this adds ten more electrons per atom, and the computational cost increases tenfold just for the 2-atom Ge calculation, and was excluded. Also, in the absence of consistent experimental reports, model parameters were not adjusted to try to fit empirical data for  $\text{Ge}_{1-x}\text{C}_x$ .

## RESULTS

### 0.78% Carbon

Figure 2 shows the folded band structure of  $\text{Ge}_{0.9922}\text{C}_{0.0078}$ . This C concentration is obtained using a 128 atom supercell, with 127 Ge atoms and 1 C atom. The computational lattice constant is 5.6854 Å, a decrease consistent with Vegard’s law from the Ge computational lattice constant of 5.6953 Å. This figure clearly shows a strongly direct bandgap, with similar conduction and valence band effective masses, and with similar shapes between the  $E^+$  and  $E^-$  conduction bands at  $\Gamma$ . Consistent with the anticrossing discussion in “Introduction” section, the C has strongly perturbed the energies at the Brillouin zone center and driven the lowest conduction band valley to much lower energy at  $\Gamma^{11}$  while the energies at  $L$  and  $X$  remain relatively unperturbed.

### 1.85% Carbon

Figure 3 shows the folded band structure for  $\text{Ge}_{0.9815}\text{C}_{0.0185}$ , a supercell with 53 Ge atoms and 1 C atom. The new computational lattice constant is 5.6619 Å. For this concentration of C, the lowest

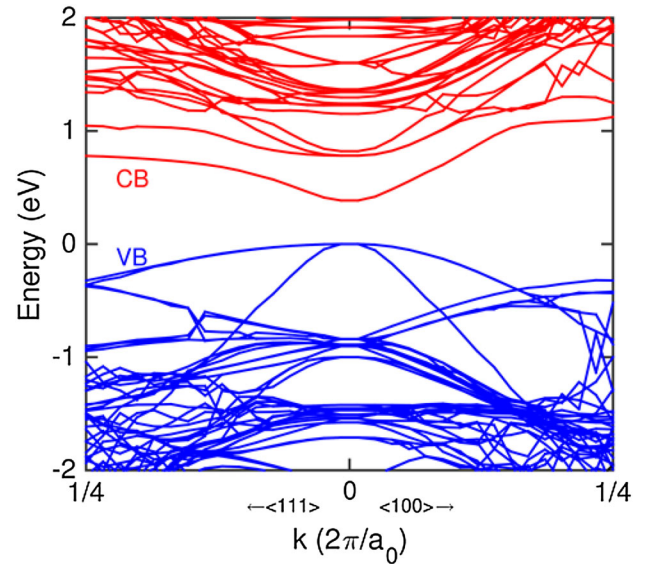


Fig. 2. Folded band structure of 128-atom  $\text{Ge}_{0.9922}\text{C}_{0.0078}$  with HSE06 but without SOC. This clearly shows a direct bandgap. CB (red online) represents the conduction bands and VB (blue online) the valence bands (Color figure online).

conduction band at  $\Gamma$  is driven to the point of just crossing the valence band. Careful inspection of the energy at the  $L$  valley shows a much smaller decrease in energy than at  $\Gamma$ , supporting the BAC model of strong interaction at the  $\Gamma$  valley.

### 6.25% Carbon

Figure 4 shows the folded band structure for  $\text{Ge}_{0.9375}\text{C}_{0.0625}$ . This composition was obtained using a supercell containing 16 atoms: 15 Ge and 1 C. The new computational lattice constant is 5.5744 Å. With 6.25% C, the lowest conduction band is driven down in energy far enough to cross the valence bands, characteristic of conducting metals. The incorporated C has decreased the energy of the  $\Gamma$  conduction band valley dramatically. This concentration of C, however, is beyond the level of a small perturbation. As is shown in the bandstructures below, the band edges have become strongly

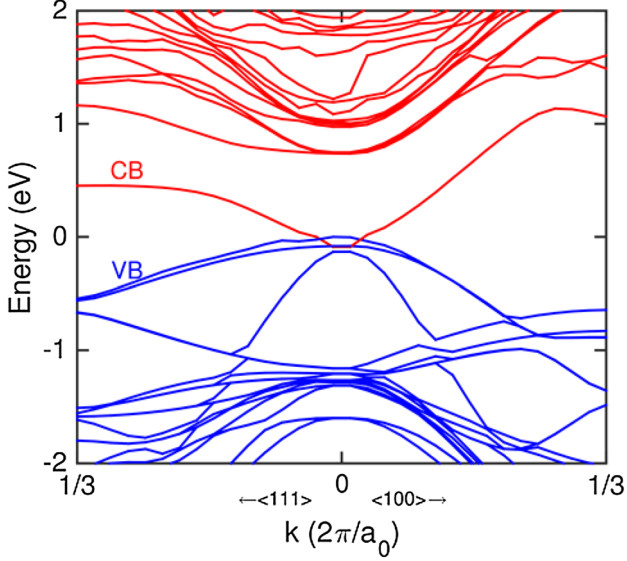


Fig. 3. Folded band structure of 54-atom  $\text{Ge}_{0.9815}\text{C}_{0.0185}$  with HSE06 but without SOC. There is no bandgap present.

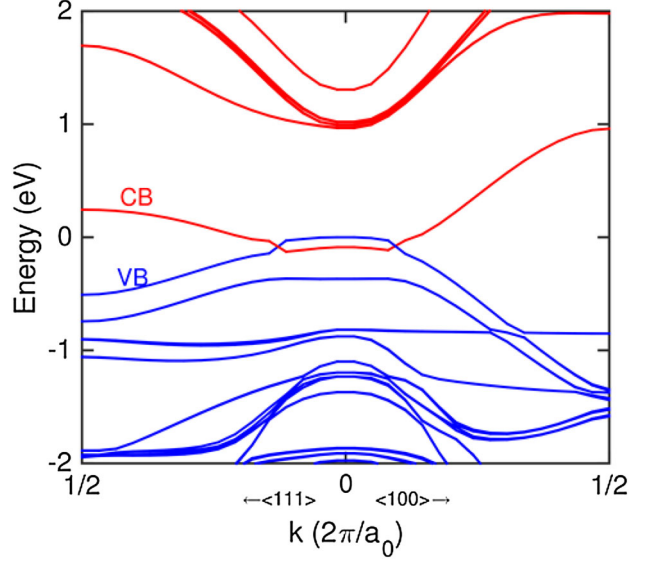


Fig. 5. Folded band structure of 16-atom  $\text{Ge}_{0.9375}\text{C}_{0.0625}$  with HSE06 and SOC. Note better convergence of valence band structure with SOC.

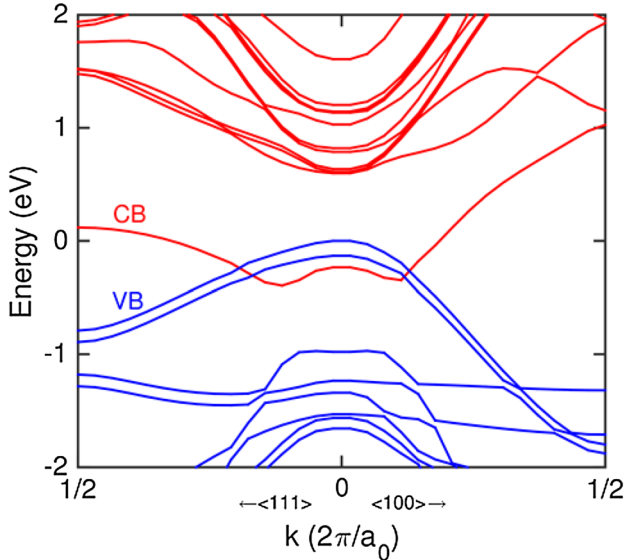


Fig. 4. Folded band structure of 16-atom  $\text{Ge}_{0.9922}\text{C}_{0.0078}$  with HSE06 but without SOC.

distorted in shape and are no longer approximately parabolic. Being strongly metallic, this concentration of C is also far too high for traditional, light-emitting optoelectronic materials.

To validate whether SOC would significantly affect the band structure, the band structure for this simplest cell was also calculated with SOC. As shown in Fig. 5, the valence bands are better resolved, showing more pronounced changes in hole effective masses and spin-orbit splitting. These differences will be important for calculating device level characteristics, but they do not significantly affect the fundamental bandgap, which is the main

purpose of this work. A detailed examination of SOC for larger supercells (lower at.% C) is beyond the scope of this paper and will be presented elsewhere.

## DISCUSSION

Table I summarizes the changes in band edge energies with percent C. The valence band maximum has been set to zero. For the 16-atom cell, the  $\Gamma$  valley minimum is taken from a parabolic fit of the valley. The bandgap changes as  $(-170 \text{ meV} \pm 50)/\%C$  for the first percent C. This decrease in the direct bandgap at  $\Gamma$  is consistent with results from similar highly mismatched alloys (as much as 200 meV reduction in bandgap for 1% N in GaAs<sup>29</sup>) and the BAC model. The energies at the  $L$  point and the minimum in the  $X$  direction were determined after unfolding the band structure using the method described by Tomić et al.<sup>30</sup>

In addition, the lowest  $L$  valley does not appear to change as quickly with increasing C content. Taking into account the slight underestimation of the bandgap at  $\Gamma$ ,  $\text{Ge}_{1-x}\text{C}_x$  should become direct bandgap for  $x > 0.008$ . Interpolation of  $E_{g\Gamma}$  indicates that  $\text{Ge}_{1-x}\text{C}_x$  becomes metallic ( $E_g < 0$ ) for  $x > 0.017$ . There is still some uncertainty in this result given the bandgap at  $\Gamma$  is slightly underestimated for Ge and the lack of SOC data for 54- and 128-atom supercells. Furthermore, the actual bandgap should be compared with results from  $\text{Ge}_{1-x}\text{C}_x$  grown by techniques that minimize C clusters. A novel technique that involves custom precursor gases where the C atoms are surrounded and bonded to Ge atoms before they are incorporated into the lattice is currently being investigated, and these measurements are underway. Although, by its nature, this simulation assumes periodic ordering of



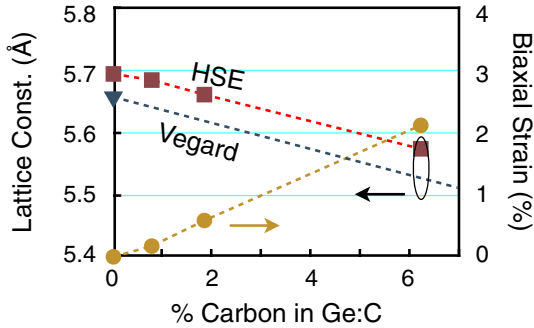


Fig. 6. Computational lattice constant with increasing C content (top, dashed line) agrees well with Vegard’s law with 2% offset from experimental values (lower, dotted line). The associated biaxial tensile strain of  $\text{Ge}_{1-x}\text{C}_x$  on a Ge template is also shown.

the C atoms for computational feasibility, proper growth conditions favor carbon atoms no closer than the third nearest neighbors.<sup>18</sup> This means that the carbon atoms will have less interaction with each other, and the alloy is not completely random.

It is noteworthy that the BAC model provides a reasonable fit to the lowest two conduction bands only near  $\Gamma$  or along  $\langle 111 \rangle$  toward  $L$ . Figures 2 and 3 show the lowest CB approaching a horizontal asymptote in the  $L$  direction, as predicted by the BAC model. However, along  $\langle 100 \rangle$  toward  $X$ , the CB clearly crosses this asymptote as well as the energies of the next higher conduction bands ( $E^+$ ). This indicates that the interaction parameter  $V$  in the BAC model is not constant with  $\vec{k}$ , but varies anisotropically as a function of  $\vec{k}$ .

At  $L$ , two distinct bands can be identified as  $E^+$  and  $E^-$ . This allows us to tentatively identify the energy of the carbon isoelectronic impurity level as  $E_C = (E^+ + E^-)/2 = 1.06 \pm 0.19$  eV above the valence band maximum.

VASP overestimates the lattice constant for Ge by 0.66%. As we would expect due to C being a smaller atom, the calculated lattice constants of the  $\text{Ge}_{1-x}\text{C}_x$  cells decrease linearly with increasing C content, as shown in Fig. 6. The lattice constants follow Vegard’s law, following a straight line between Ge and C, in contrast to predictions by Kelires et al.<sup>18</sup>

While this study only seeks to explore the characteristics of relaxed  $\text{Ge}_{1-x}\text{C}_x$  films, tensile strain is actually advantageous for further decreasing the direct bandgap, as mentioned above. The right axis in Fig. 6 shows biaxial tensile strain that would occur in the  $\text{Ge}_{1-x}\text{C}_x$  layer if it were grown on Ge. The 54-atom supercell, with 1.85% C, would have about 1% biaxial tensile strain if grown on Ge. 0.78% C should be stable for bulk growth as the critical thickness is approximately 160 nm. Adding small amounts of Sn would allow strain compensation while also enhancing the direct bandgap of the alloy.

One of the issues with tensile-strained Ge for light emission is the low occupation of electrons in the  $\Gamma$  valley. Even with 2% biaxial tensile strain,

enough to turn Ge into a direct bandgap, only 2.5–6% of electrons are in the  $\Gamma$  valley.<sup>32,33</sup> Band anticrossing has the advantage for light emitters of increasing the effective mass in the  $\Gamma$  valley.<sup>34</sup> As the lower conduction band valley is repelled and driven down in energy at  $\Gamma$ , the effective mass increases. This increase leads to higher occupation at  $\Gamma$ , a closer match between  $m_e^*$  and  $m_h^*$ , and therefore stronger recombination across the direct bandgap. This strongly suggests  $\text{Ge}_{1-x}\text{C}_x$  as a preferred laser material over tensile-strained Ge.

## CONCLUSIONS

In conclusion, we computed the band structure of  $\text{Ge}_{1-x}\text{C}_x$  alloys using ab initio hybrid exchange density functional techniques.  $\text{Ge}_{1-x}\text{C}_x$  was found to be promising as a direct bandgap Group IV alloy for Si-based lasers, photodetectors, and solar cells. The band structures showed a striking reduction in  $E_{g\Gamma}$  with increasing carbon content, estimated at  $(170 \text{ meV} \pm 50)/\%C$  for the first percent C, consistent with band anticrossing behavior at  $\vec{k} = 0$ . The band structure away from zone center ( $\vec{k} \gg 0$ ) was inconsistent with a constant interaction potential in the BAC model. However, a smaller change in the  $L$  valley energy suggests that the symmetry of the C isoelectronic impurity primarily affects the  $\Gamma$  valley, leading to a direct bandgap. Also, smaller 16-atom supercells show that spin-orbit coupling induces important changes for device characterization near  $\vec{k} = 0$ , particularly the effective mass of light holes and spin-orbit splitting that are crucial for lasers and modulators. Future improvements would examine the role of biaxial strain and defects, as well as including SOC for the large supercells. These efforts are currently underway.

## ACKNOWLEDGEMENTS

This work was supported by the National Science Foundation (NSF) under Grants CBET-1438608 and DMR-1508646 and the Extreme Science and Engineering Discovery Environment (XSEDE) supported by NSF Grant number ACI-1053575. This research was also supported in part by the Notre Dame Center for Research Computing, with valuable assistance from Dodi Heryadi. The authors thank Vince Lordi and Eoin O’Reilly for helpful discussions.

## REFERENCES

1. J. Liu, X. Sun, R. Camacho-Aguilera, L.C. Kimerling, and J. Michel, *Opt. Lett.* 35, 679 (2010).
2. N. Pavarelli, T.J. Ochalski, F. Murphy-Armando, Y. Huo, M. Schmidt, G. Huyet, and J.S. Harris, *Phys. Rev. Lett.* 110, 177404 (2013).
3. M. de Kersauson, M. El Kurdi, S. David, X. Checoury, G. Fishman, S. Sauvage, R. Jakomin, G. Beaudoin, I. Sagnes, and P. Boucaud, *Opt. Express* 19, 17925 (2011).
4. D. Nam, D. Sukhdeo, S.-L. Cheng, A. Roy, K.C.-Y. Huang, M. Brongersma, Y. Nishi, and K. Saraswat, *Appl. Phys. Lett.* 100, 131112 (2012).

5. R.E. Camacho-Aguilera, Y. Cai, N. Patel, J.T. Bessette, M. Romagnoli, L.C. Kimerling, and J. Michel, *Opt. Express* 20, 11316 (2012).
6. M. Qi, W.A. O'Brien, C.A. Stephenson, N. Cao, B.J. Thibeault, and M.A. Wistey, *6th International Silicon-Germanium Technology Device Meeting (ISTDM 2012)* (Berkeley, CA, 2012).
7. H.H. Tseng, K.Y. Wu, H. Li, V. Mashanov, H.H. Cheng, G. Sun, and R.A. Soref, *Appl. Phys. Lett.* 102, 182106 (2013).
8. J.P. Gupta, N. Bhargava, S. Kim, T. Adam, and J. Kolodzey, *Appl. Phys. Lett.* 102, 251117 (2013).
9. S. Gupta, B. Magyari-Köpe, Y. Nishi, and K.C. Saraswat, *J. Appl. Phys.* 113, 053707 (2013).
10. R. Chen, H. Lin, Y. Huo, C. Hitzman, T.I. Kamins, and J.S. Harris, *Appl. Phys. Lett.* 99, 181125 (2011).
11. W. Shan, W. Walukiewicz, J.W. Ager III, E.E. Haller, J.F. Geisz, D.J. Friedman, J.M. Olson, and S.R. Kurtz, *Phys. Rev. Lett.* 82, 1221 (1999).
12. S.R. Bank, H. Bae, L.L. Goddard, H.B. Yuen, M.A. Wistey, R. Kudrawiec, and J.S. Harris, *IEEE J. Quantum Electron.* 43, 773 (2007).
13. M. Okinaka, K. Miyatake, J. Ohta, and M. Nunoshita, *J. Cryst. Growth* 255, 273 (2003).
14. J. Kolodzey, P.R. Berger, B.A. Orner, D. Hits, F. Chen, A. Khan, X. Shao, M.M. Waite, S.I. Shah, C.P. Swann, and K.M. Unruh, *J. Cryst. Growth* 157, 386 (1995).
15. K.J. Roe, M.W. Dashiell, J. Kolodzey, P. Boucaud, and J.-M. Lourtioz, *J. Vac. Sci. Technol., B* 17, 1301 (1999).
16. D. Gall, J. D'Arcy-Gall, and J. Greene, *Phys. Rev. B* 62, R7723 (2000).
17. C. Guedj, J. Kolodzey, and A. Hairie, *Phys. Rev. B* 60, 150 (1999).
18. P. Kelires, *Phys. Rev. B* 60, 10837 (1999).
19. J. D'Arcy-Gall, D. Gall, I. Petrov, P. Desjardins, and J.E. Greene, *J. Appl. Phys.* 90, 3910 (2001).
20. G. Kresse and J. Hafner, *Phys. Rev. B* 47, 558 (1993).
21. G. Kresse and J. Hafner, *Phys. Rev. B* 49, 14251 (1994).
22. G. Kresse and J. Furthmüller, *Phys. Rev. B* 54, 11169 (1996).
23. G. Kresse and J. Furthmüller, *Comput. Mater. Sci.* 6, 15 (1996).
24. P. Blöchl, *Phys. Rev. B* 50, 17797 (1994).
25. G. Kresse and D. Joubert, *Phys. Rev. B* 59, 1758 (1999).
26. J.P. Perdew, K. Burke, and M. Ernzerhof, *Phys. Rev. Lett.* 77, 3865 (1996).
27. J.P. Perdew, K. Burke, and M. Ernzerhof, *Phys. Rev. Lett.* 78, 1396 (1997).
28. A.V. Krukau, O.A. Vydrov, A.F. Izmaylov, and G.E. Scuseria, *J. Chem. Phys.* 125, 224106 (2006).
29. G. Stenuit and S. Fahy, *Phys. Rev. B* 76, 035201 (2007).
30. M. Tomić, H. Jeschke, and R. Valentí, *Phys. Rev. B* 90, 195121 (2014).
31. L.E. Vorobyev, *Handbook Series Semiconductor Parameters*, vol. 1, ed. M. Levinshtein, S. Rumyantsev, and M. Shur (Singapore: World Scientific Publishing Co Pte Ltd, 1996), p. 33.
32. G.-E. Chang and H.H. Cheng, *J. Phys. D* 46, 065103 (2013).
33. M. Virgilio, C.L. Manganelli, G. Grosso, G. Pizzi, and G. Capellini, *Phys. Rev. B* 87, 235313 (2013).
34. P.R.C. Kent, L. Bellaiche, and A. Zunger, *Semicond. Sci. Technol.* 17, 851 (2002).